Received 16 November 2023; revised 3 January 2024; accepted 9 January 2024. Date of publication 15 January 2024; date of current version 6 August 2024.

Digital Object Identifier 10.1109/OJAP.2024.3353810

A Dual-Beam Filtering Antenna Based on Dual-Mode Patch Loaded With π-Shaped Vias

LINGYAN ZHANG [1,2,3], TIANNAN NI [1], JIN SHI [1,2,3] (Member, IEEE), GU LIU [1], AND KAI XU [1,2,3] (Member, IEEE)

[1]School of Information Science and Technology, Nantong University, Nantong 226019, China

[2]Research Center for Intelligent Information Technology, Nantong University, Nantong 226019, China

[3]Nantong Key Laboratory of Advanced Microwave Technology, Nantong University, Nantong 226019, China

CORRESPONDING AUTHOR: J. SHI (e-mail: jinshi0601@hotmail.com)

This work was supported in part by the National Natural Science Foundation of China under Grant 52101017, Grant 62201291, and Grant 62201292; in part by the Key Research and Development Program of Jiangsu Province of China under Grant BE2021013-1; in part by the Nantong Science and Technology Plan Project under Grant JB2021006; and in part by the Natural Science Research Project of Jiangsu Higher Education Institutions under Grant 21KJD430001 and Grant 22KJB140004.

ABSTRACT In this paper, a dual-beam filtering patch antenna is proposed, wherein a symmetrical π-shaped metal vias-loaded dual-mode patch and a cross-shaped metal strip are utilized. The dual-mode patch resonator is realized through the loading of metal vias in the weak field region of mode TM_{21}, which effectively moves mode TM_{01} closer to TM_{21}. Using a cross-shaped metal strip to excite the dual-mode patch resonator not only provides a reflection zero and broadens the bandwidth, but also generates two radiation nulls through zero coupling, thus improving the frequency selectivity. Compared with reported dual-beam filtering patch antenna, the proposed design with the novel dual-mode patch resonator has a wide stopband, enhanced frequency selectivity, small size and a low profile. Measurements show that the antenna exhibits a 10-dB impedance matching bandwidth of 13% (3.23 GHz – 3.69 GHz), with two radiation nulls at 3.15 GHz and 3.88 GHz and a measured 15 dB stopband of 2.14 f_0.

INDEX TERMS Dual-beam, filtering patch antenna, frequency selectivity, wide stopband.

I. INTRODUCTION

DUE TO their ability to provide larger data capacities and reduce multipath and interference effects, dual-beam antennas are currently under intense research focus, especially for the design of wireless systems that require fewer antennas, such as micro base stations, vehicle communication systems, satellite communication systems, etc. [1], [2], [3], [4]. Filtering antennas are also receiving more attention from researchers, as they can not only reduce the size of the systems employing them, but also the distance between systems operated at different frequencies [5], [6], [7], [8], [9], [10]. Dual-beam filtering patch antennas (DBFPAs) combine these two advantages with light weight and low cost and thus exhibit significant research value.

Most reported dual-beam patch antenna studies do not take into account potential filtering functions [11], [12], [13], [14], [15] and are realized through the TM_{02} mode [1], while T- or cross-shaped probes are used to realize dual-beam radiation [11], [16].

A few dual-beam patch antennas with filtering functions have been proposed [17], [18], [19]. In [17], a pair of T-shaped metallic strip was loaded to generate a wide operating band with a symmetrical dual-beam radiation pattern, while two reflective radiation nulls were generated in both the upper and the lower stopbands. Although the fusion of filtering and dual-beam radiation was realized, the antenna's frequency selectivity and stopband bandwidth need to be further improved. In [18], a DBFPA with two radiation nulls near the edges of the operating band was implemented using a metal strip and a patch with two symmetrical slots. This configuration showed improved frequency selectively as well as a wide stopband.

In this paper, by utilizing a cross-shaped metal strip to feed a dual-mode π-shaped vias-loaded patch resonator, a compact DBFPA with high frequency selectivity and wide

© 2024 The Authors. This work is licensed under a Creative Commons Attribution-NonCommercial-NoDerivatives 4.0 License.
For more information, see https://creativecommons.org/licenses/by-nc-nd/4.0/

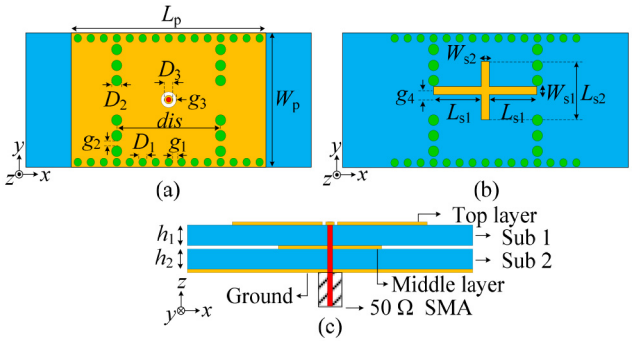

FIGURE 1. Structural schematic diagram of dual-beam filtering patch antenna. (a) Top-layer structure. (b) Middle-layer structure. (c) Cross-section view.

stopband is proposed. Three reflection zeros are obtained from two modes of the patch resonator and one equivalent L-C mode of the metal strip cure, while two radiation nulls are generated through the zero coupling of electric fields. The evolution process, electric field distribution, and the resonant frequency of the proposed dual-mode patch resonator are given in detail. The analysis of the controllable reflection zero and radiation nulls is verified through an analysis of the electric field distribution and a parametric study. Finally, a prototype of the proposed DBFPA is designed, fabricated, measured and evaluated against state-of-the-art approaches.

II. ANTENNA DESIGN

A. ANTENNA CONFIGURATION

Figure 1 is a schematic diagram of the proposed DBFPA loaded with π-shaped vias. As can be seen from Figure 1, the proposed antenna is mainly composed of a rectangular holed patch on the top layer, a cross-shaped metal strip on the middle layer, and a ground on the bottom layer. The top rectangular metal patch is connected to the metal earth through a pair of π-shaped metallized vias which are symmetrical. The inner conductor of the SMA connector connects the cross-metal strip in the middle layer and the top metal patch. The dielectric substrates 1 and 2 are Rogers RO4003C substrates ($\varepsilon_r = 3.55$, $\tan\delta = 0.0027$) with thicknesses of $h_1 = 1.524$ mm and $h_2 = 1.624$ mm, respectively.

B. ANALYSIS OF THE π-SHAPED VIAS-LOADED PATCH RESONATOR

Figure 2(a) shows the structural diagram of the traditional patch-loaded metal resonator, which includes both row- and column-vias. As can be seen from Figure 2(b) and 2(c), the first mode of the resonator is TM_{01}, the field under the patch is in the same direction, and the electric field component at the edge of the opening is reversed along the x direction, which facilitates the generation of radiation along two directions. In the second mode, TM_{21}, the electric field below the patch presents a wavelength distribution along the x direction, and the electric field components at the edge of the opening are also reversed along the x direction, resulting in radiation in two directions.

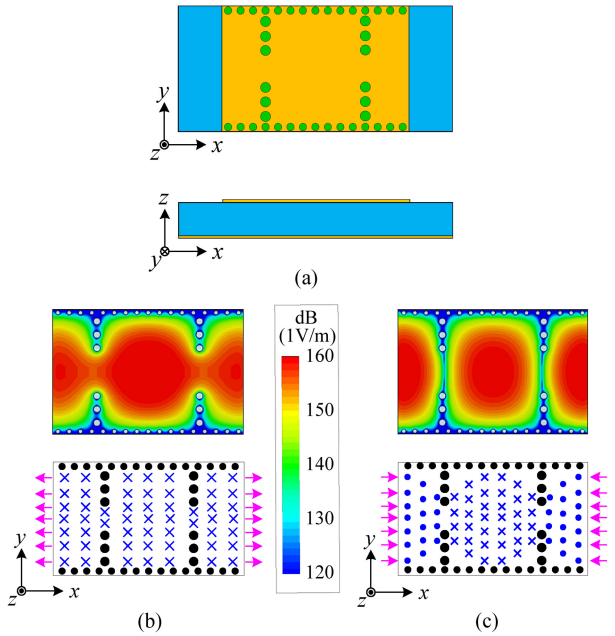

FIGURE 2. The structure diagram, average amplitude electric field diagram and electric field schematic diagram of π-shaped vias-loaded patch resonator. (a) The structure diagram of patch resonator loaded with π-shaped vias. The average amplitude electric field diagram and electric field schematic diagram of (b) TM_{01} mode and (c) TM_{21} mode.

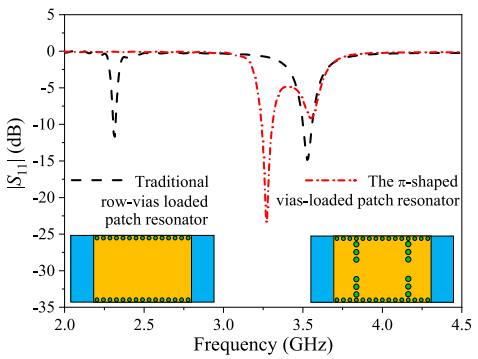

FIGURE 3. Simulated S-parameters of the patch resonator.

Figure 3 shows the S-parameter responses of the traditional and the proposed resonators when fed using probes. It is evident that the resonant frequency of mode TM_{01} is shifted up to form a radiation band with mode TM_{21}.

In order to determine the resonant frequency of the proposed π-shaped vias-loaded resonator, the main parameters of the metal-through vias were studied, as shown in Figure 4. It can be seen that with the increase of *dis*, the resonant frequency of mode TM_{01} first increases and then decreases, while the resonant frequency of TM_{21} and the distance between the two modes first decrease and then increase. As can be seen from Figure 4(b), with the increase of g_2, the resonant frequency of TM_{01} increases, while the resonant frequency of TM_{21} remains unchanged and the distance between the two modes decreases. As can be seen from Figure 4(c), with the increase of D_2, the

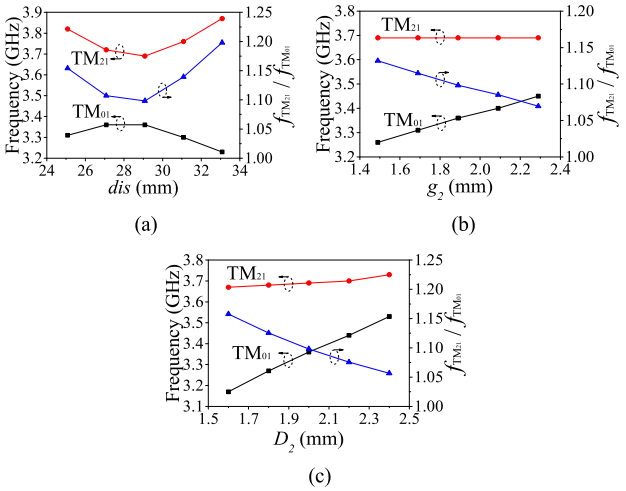

FIGURE 4. Simulated resonator frequency and ratio of resonator frequency of the proposed patch resonator under different parameters. (a) Different *dis*. (b) Different g_2. (c) Different D_2.

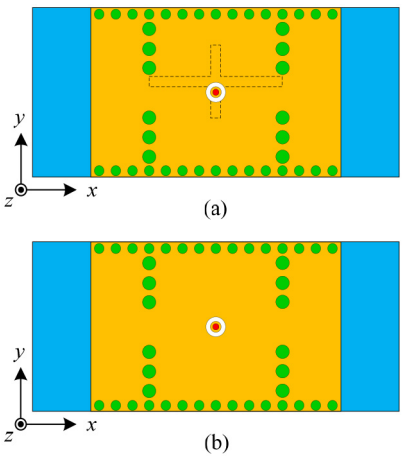

FIGURE 5. The structure diagram of the proposed antenna and that without the cross-shaped metal strip. (a) π-shaped vias-loaded patch antenna. (b) π-shaped vias-loaded patch antenna with cross-shaped metal stripline.

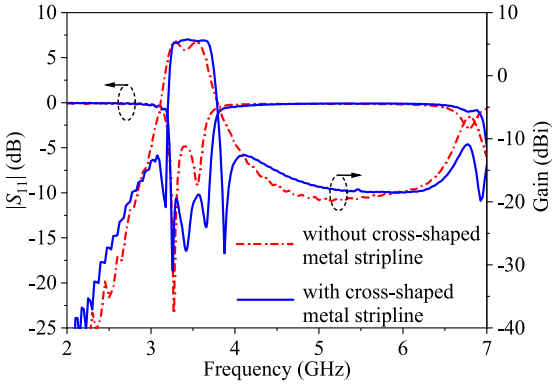

FIGURE 6. Simulated S-parameters of the patch antenna.

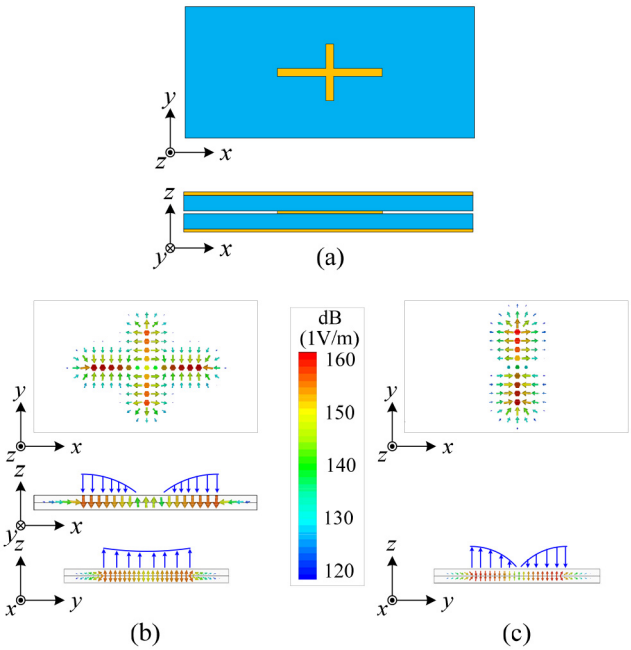

FIGURE 7. The structure diagram and vector electric fields diagram of the cross-shaped metal strip resonator. (a) The structure diagram of the cross-shaped stripline resonator. The vector electric field schematic diagram of (b) the first mode and (c) the second mode.

resonant frequencies of the two modes increase, with the resonant frequency of TM_{01} increasing more rapidly, while the distance between the two modes decreases. Therefore, in the proposed π-shaped vias-loaded patch resonator, the resonant frequencies of TM_{01} and TM_{21} and the distance between the resonant frequencies of the two modes can be adjusted using *dis*, g_2 and D_2.

C. ANTENNA OPERATING MECHANISM

To establish the operating mechanism of the proposed antenna, the proposed configuration with cross-shaped metal strips, shown in Figure 5(a), was compared with a configuration without a cross-shaped metal strip, shown in Figure 5(b). The performance of the compared configurations is shown in Figure 6. It can be found that the addition of the cross-shaped metal strips on the middle layer, results in the addition of one reflection zero in the operating band and a bandwidth increase. Additionally, two radiation nulls occur near the edges of the operating bands, which improves the frequency selectivity effectiveness.

Figure 7(a) shows the structure of the cross-shaped metal strip resonator, which consists of a rectangular metal patch at the top layer, a cross-shaped metal structure at the middle layer, a first substrate, a second substrate and a metal ground. The vector electric fields of the two resonator modes are shown in Figure 7(b) and 7(c). It can be seen from Figure 7(b) that when the cross-shaped stripline resonator operates in the first mode, the electric fields are mainly concentrated on the horizontal and vertical metal strips, and the electric fields on both sides of the strips are larger than those in the middle. The electric fields on the left and right parts of the horizontal metal strip all show quarter-wavelength distribution and have the same direction. The electric fields on the left and right parts of the vertical

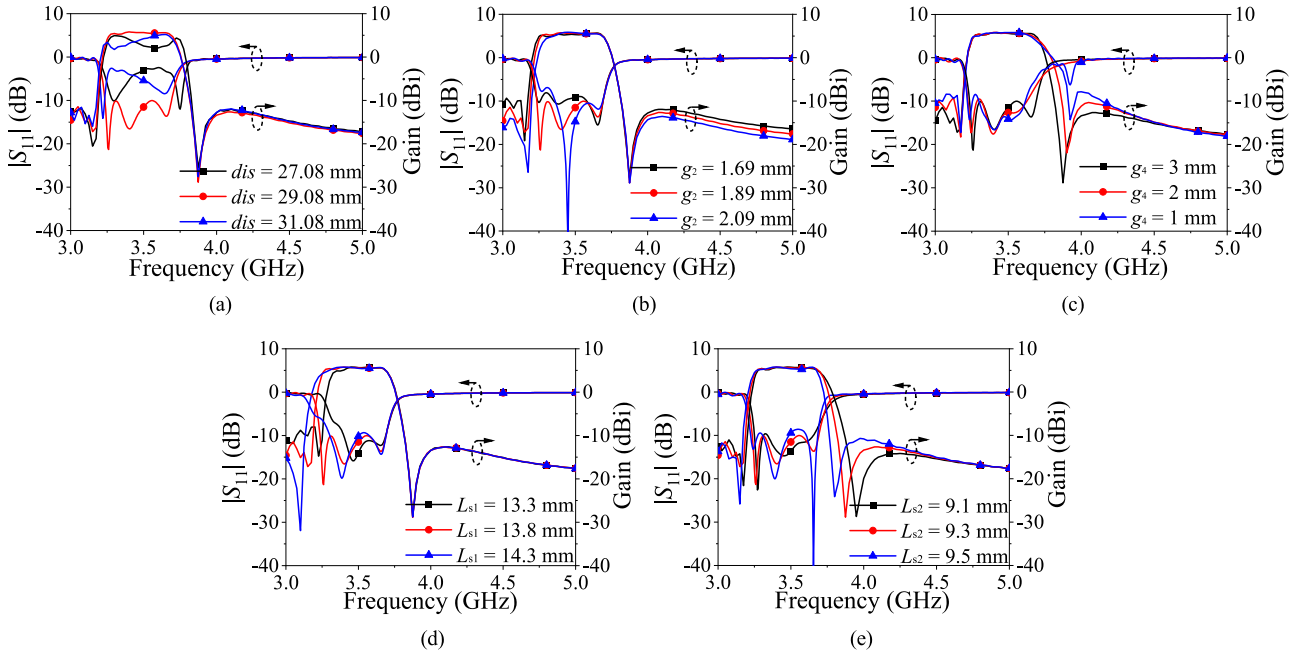

FIGURE 8. Simulated S-parameters and Gain of the proposed antenna. (a) Different widths of the vias *dis*. (b) Different distances of the vias g_2. (c) Different distances from the center of the cross-strip g_4. (d) Different lengths of the cross-strip L_{s1}. (e) Different widths of the cross-strip L_{s2}.

metal strip are symmetrically distributed, while those of the horizontal strip are opposite. As can be seen from Figure 7(c), when the cross-stripline resonator operates in the second mode, the electric field is mainly concentrated on the vertical metal strip, and there is almost no electric field on the horizontal one. The field on the vertical strip presents a half-wave distribution, and the field on the upper part of the strip has the same amplitude and the opposite direction as that in the lower part.

Due to the two modes of the cross-shaped metal stripline, the overall integration of the electric field is zero for the operating modes of the π-shaped vias-loaded patch antenna. This results in the two radiation nulls of Figure 6 and consequently the filtering effect of the antenna. In addition, the equivalent capacitance is formed between the top metal patch and the cross-shaped metal strip, the equivalent inductance is formed on the first substrate of the SMA connector, and the equivalent resonance between the top metal patch and the cross-shaped metal strip generates the first reflection zero in the band, which expands the operational bandwidth of the antenna.

D. PARAMETRIC STUDY ON DIS, G_2, G_4, L_{S1} AND L_{S2}

In order to clarify the influence of the antenna's physical parameters on $|S_{11}|$ and its gain, five parameters, namely the distance between the two vertically arranged vias (*dis*), the distance between the vertically arranged metallized vias (g_2), the vertical position of the cross-shaped metal strip in the middle layer (g_4), the length of the horizontal metal strip in the middle layer (L_{s1}) and the length of the vertical metal strip in the middle layer (L_{s2}), were analyzed, as shown in Figure 8.

It can be seen from Figure 8(a) that the impedance matching performance of the antenna is first improved and then deteriorates with the increase of *dis*, because when *dis* = 29.08 mm, the metallized via is located in the zero electric field region of mode TM_{21}, which has little influence on the antenna's matching performance. Figure 8(b) shows that the antenna bandwidth decreases as g_2 is increased, because the resonant frequencies of TM_{01} and TM_{21} increase. It can be seen from Figure 8(c) that the impedance-matching performance of the antenna changes with g_4 because the input impedance of the antenna changes with the vertical movement of the cross-shaped metal strip. It is also evident from Figure 8(d) and 8(e) that the low- and high-frequency radiation nulls of the antenna move up with the decrease of L_{s1} and L_{s2}, respectively, because the resonant frequencies of the two modes of the cross-shaped stripline resonator increase.

E. ANTENNA DESIGN PROCESS

Based on the above analysis, the summary of the proposed antenna design process is as follows:

1) The operational frequency f_0, the bandwidth and the radiation null frequency of the DBFPA are set.

2) The initial dimensions L_p and W_p of the metal patch are obtained by setting $f_{TM21} = f_0$. The widths of the vias *dis*, the vias' diameter D_2, and distances of the vias g_2 of the middle two columns can be obtained from the variation rule shown in Figure 4.

3) The length of the horizontal metal strip L_{s1} and the length of the vertical metal strip L_{s2} are initially set according to the radiation null frequency.

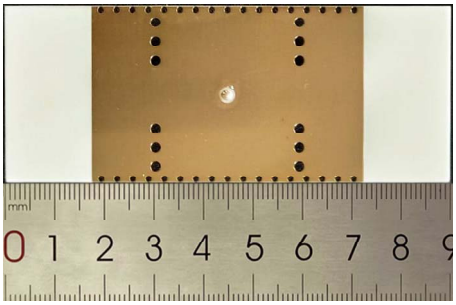

FIGURE 9. Photograph of the π-shaped vias-loaded patch antenna.

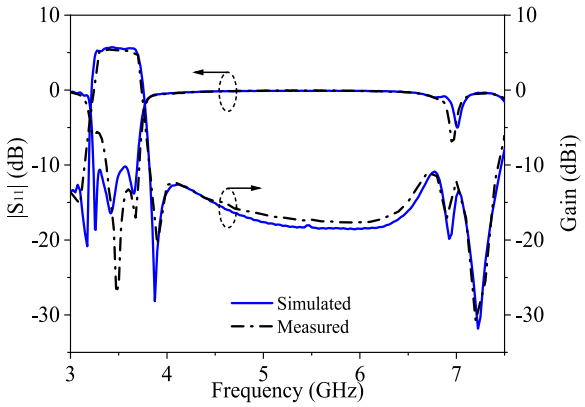

FIGURE 10. Simulated and measured results of the proposed π-shaped vias-loaded patch antenna.

4) Using the variation rule in Figure 8 and the set operating frequency, bandwidth and radiation nulls, L_{s1}, L_{s2}, D_1, g_1, D_3 and g_3 are fine-tuned in the full-wave simulation to obtain the final antenna size.

III. RESULTS

Figure 9 is a photograph of a prototype of the proposed DBFPA. The detailed dimensions of the antenna were as follows: $l_g = 90$ mm, $w_g = 36$ mm, $l_p = 55$ mm, $w_p = 36$ mm, $d = 27.08$ mm, $D_v = 2$ mm, $g_v = 1.89$ mm, $l_s = 29.5$ mm, $l_{s1} = 19.1$ mm, $w_s = 0.5$ mm, $w_{s1} = 1.9$ mm, $h_1 = 1.524$ mm, and $h_2 = 1.624$ mm. The S-parameters of the fabricated antenna were measured on a Keysight N5227A network analyzer. The radiation performance was measured in an anechoic chamber using a far-field antenna measurement system.

The simulated and measured $|S_{11}|$ and gain of the prototype are shown in Figure 10. The measured 10-dB impedance matching bandwidth was 13% (3.23 GHz – 3.69 GHz). The measured gain of the bandwidth was flat and greater than 5.2 dBi. Two radiation nulls occurred at 3.15 GHz and 3.88 GHz, respectively. The measured 15 dB stopband was up to 2.14 f_0, while the 20-dB roll-off coefficient (ξ) was 170, calculated using:

$$\xi = \left| \frac{G_{\Delta 20\mathrm{dB}} - G_{\Delta 3\mathrm{dB}}}{f_{\Delta 20\mathrm{dB}} - f_{\Delta 3\mathrm{dB}}} \right| \quad (1)$$

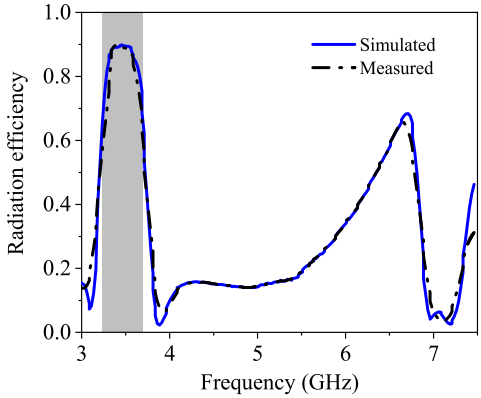

FIGURE 11. The simulated and measured radiation efficiency of the proposed antenna.

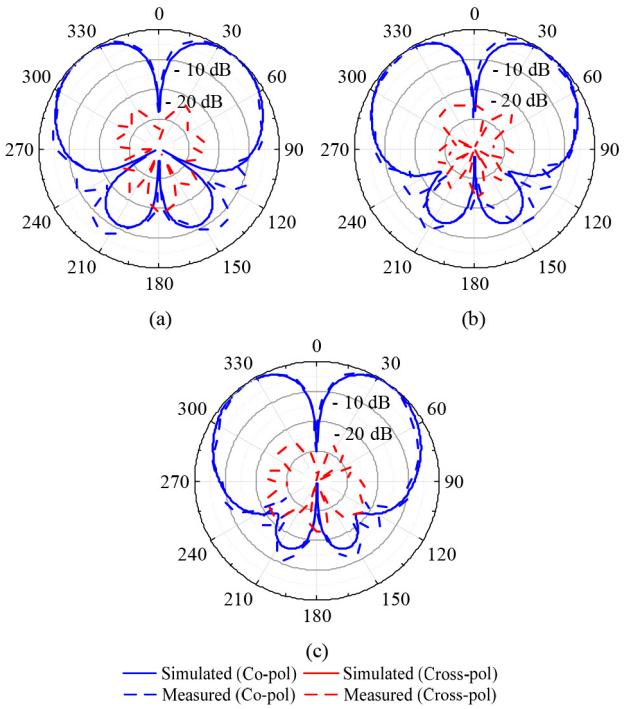

FIGURE 12. The simulated and measured radiation patterns of the proposed antenna. (a) 3.26 GHz, (b) 3.42 GHz, (c) 3.66 GHz.

where $G_{\Delta 20dB}$ and $G_{\Delta 3dB}$ are the gain values which are reduced by 20-dB and 3-dB respectively compared with the gain in the operating frequency band, and $f_{\Delta 20dB}$ and $f_{\Delta 3dB}$ are the frequencies corresponding to $G_{\Delta 20dB}$ and $G_{\Delta 3dB}$, respectively.

Figure 11 shows the simulation and measured efficiency curves of the proposed antenna. It can be seen that the measured peak radiation efficiency in the operating frequency band is about 90%.

Figure 12 exhibits the simulated and measured radiation patterns at three frequencies (3.26 GHz, 3.42 GHz and 3.66 GHz). It can be seen that the two main radiation beams at the three frequencies were both directed at Phi = 0° and

TABLE 1. Performance summary of the proposed and state-of-the-art designs.

Ref.	f_0 (GHz)	Antenna dimensions ($\lambda_0 \times \lambda_0 \times \lambda_0$)	FBW (%)	Radiation efficiency (%)	Rejection up to 15dB	ξ	Filtering
[1]	5.49	$0.62 \times 0.49 \times 0.058$	11.3	95	-	-	N
[2]	5.46	$0.77 \times 0.44 \times 0.10$	13.2	N.A.	-	-	N
[16]	2.40 / 5.25	$0.81 \times 0.59 \times 0.17$	7.3 / 12.7	N.A.	-	-	N
[17]	5.38	$0.8 \times 0.46 \times 0.043$	19.3	75	$1.39\,f_0$	28	Y
[18]	3.5	$0.8 \times 0.4 \times 0.096$	23.5	N.A.	$2\,f_0$	113	Y
This work	3.5	$0.64 \times 0.42 \times 0.037$	13	90	$2.14\,f_0$	170	Y

Theta $= \pm 39°$. The measured cross-polarization levels were all lower than -20 dB.

Table 1 compares the proposed and state-of-the-art dual-beam patch antennas. Compared with the designs of [1], [2], and [16], the proposed one achieves the filtering function with a wide stopband. Compared with the DBFPAs [17], [18], the proposed design shows enhanced frequency selectivity, a wider stopband and has a more compact size.

IV. CONCLUSION

In this article, a DBFPA based on π-shaped vias-loaded dual-mode patch is proposed. By using a cross-shaped strip to feed the dual-mode patch, three reflection zeros and two radiation nulls are achieved simultaneously. Thus, compared with reported dual-beam patch antennas, the proposed one achieves high frequency selectivity, a wide stopband, a compact size, an excellent out-of-band suppression level and the widest stopband bandwidth.

REFERENCES

[1] A. Khidre, K.-F. Lee, A. Z. Elsherbeni, and F. Yang, "Wide band dual-beam U-slot microstrip antenna," *IEEE Trans. Antennas Propag.*, vol. 61, no. 3, pp. 1415–1418, Mar. 2013.

[2] S. Liu, S.-S. Qi, W. Wu, and D.-G. Fang, "Single-feed dual-band single/dual-beam U-slot antenna for wireless communication application," *IEEE Trans. Antennas Propag.*, vol. 63, no. 8, pp. 3759–3764, Aug. 2015.

[3] W. Yang, L. Gu, W. Che, Q. Meng, Q. Xue, and C. Wan, "A novel steerable dual-beam metasurface antenna based on controllable feeding mechanism," *IEEE Trans. Antennas Propag.*, vol. 67, no. 2, pp. 784–793, Feb. 2019.

[4] H. Ullah and F. A. Tahir, "A novel snowflake fractal antenna for dual-beam applications in 28 GHZ band," *IEEE Access*, vol. 8, pp. 19873–19879, 2020.

[5] X. Y. Zhang, W. Duan, and Y.-M. Pan, "High-gain filtering patch antenna without extra circuit," *IEEE Trans. Antennas Propag.*, vol. 63, no. 12, pp. 5883–5888, Dec. 2015.

[6] S. J. Yang, Y. M. Pan, L.-Y. Shi, and X. Y. Zhang, "Millimeter-wave dual-polarized filtering antenna for 5G application," *IEEE Trans. Antennas Propag.*, vol. 68, no. 7, pp. 5114–5121, Jul. 2020.

[7] S. Ji, Y. Dong, and Y. Fan, "Bandpass filter prototype inspired filtering patch antenna/array," *IEEE Trans. Antennas Propag.*, vol. 70, no. 5, pp. 3297–3307, May 2022.

[8] D.-S. La, C. Zhang, Y.-J. Zhang, T.-X. Jiang, M.-J. Qu, and J.-W. Guo, "A wideband filtering dielectric resonator antenna based on the $HEM_{11\delta}$ mode," *IEEE Antennas Wireless Propag. Lett.*, vol. 21, pp. 1552–1556, 2022.

[9] K. Xu, L. Jin, H. Tang, W. W. Yang, and J. Shi, "A high-efficiency dual-band self-filtering antenna based on three dense dielectric strip resonators," *IEEE Antennas Wireless Propag. Lett.*, vol. 21, pp. 1532–1536, 2022.

[10] K.-Z. Hu, H.-Y. Huang, M.-C. Tang, Z. Chen, D. Yan, and P. Wang, "A single-layer wideband differential-fed filtering antenna with high selectivity," *IEEE Trans. Antennas Propag.*, vol. 71, no. 5, pp. 4522–4527, May 2023.

[11] C. L. Mak, K. F. Lee, and K. M. Luk, "Broadband patch antenna with a T-shaped probe," *IEE Proc., Microw., Antennas Propag.*, vol. 147, no. 2, pp. 73–76, Apr. 2000.

[12] M.-Y. Li, C. T. Rodenbeck, and K. Chang, "Millimeter-wave dual-beam scanning microstrip patch antenna arrays fed by dielectric image lines," in *Proc. IEEE Antennas Propag. Soc. Int. Symp.*, 2002, pp. 196–199.

[13] R. Anand, J. A. Jose, A. M. Kaimal, and S. Menon, "Analysis of dual beam pentagonal patch antenna," in *Proc. Int. Conf. Comput. Commun. Technol.*, vol. 2, 2016, pp. 611–619.

[14] H. Lu, F. Liu, Y. A. Liu, and S. Huang, "Single-layer single-patch wideband dual-beam E-shaped patch antenna," in *Proc. IEEE Int. Symp. Electromagn. Compat. (EMC-Beijing)*, 2017, pp. 1–3.

[15] J. Tan, W. Jiang, S. Gong, T. Cheng, J. Ren, and K. Zhang, "Design of a dual-beam cavity-backed patch antenna for future fifth generation wireless networks," *IET Microw. Antenna. Propag.*, vol. 12, no. 10, pp. 1700–1703, Aug. 2018.

[16] C. Chen, Y. Guo, and H. Wang, "Wideband symmetrical cross-shaped probe dual-beam microstrip patch antenna," *IEEE Antennas Wireless Propag. Lett.*, vol. 14, pp. 622–625, 2014.

[17] J.-F. Li, C.-X. Mao, D.-L. Wu, L.-H. Ye, and G. Zhang, "A dual-beam wideband filtering patch antenna with absorptive band-edge radiation nulls," *IEEE Trans. Antennas Propag.*, vol. 69, no. 12, pp. 8926–8931, Dec. 2021.

[18] J.-F. Li, Z. N. Chen, D.-L. Wu, G. Zhang, and Y.-J. Wu, "Dual-beam filtering patch antennas for wireless communication application," *IEEE Trans. Antennas Propag.*, vol. 66, no. 7, pp. 3730–3734, Jul. 2018.

[19] W. Wang, W. Zhang, S. Ding, and Z. Zhu, "Dual-beam filtering patch antennas for millimeter-wave applications," in *Proc. IEEE MTT-S Int. Microw. Workshop Series Adv. Mater. Processes RF THz Appl. (IMWS-AMP)*, 2023, pp. 1–3.

LINGYAN ZHANG was born in Nantong, Jiangsu, China, in 1991. She received the B.Sc. degree in applied physics from Jiangsu University in 2014, and the Ph.D. degree in materials science and engineering from the Nanjing University of Science and Technology in 2019. Her research focuses on the microwave transmission system, interaction of ultrafast intense laser with semiconductors, and the surface modification of materials.

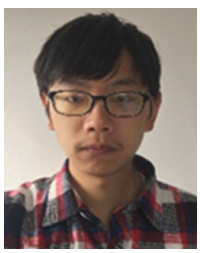

TIANNAN NI was born in Nantong, Jiangsu, China, in 1993. He received the B.S. degree from the Nanjing University of Information Science and Technology, Nanjing, Jiangsu, China, in 2016. He is currently pursuing the M.S. degree with the School of Electronics and Information, Nantong University, Nantong. His current research interest is microwave/millimeter-wave shared aperture antenna and dual-beam antenna.

JIN SHI (Member, IEEE) received the B.S. degree from Huaiyin Teachers College, Huai'an City, Jiangsu, China, in 2001, the M.S. degree from the University of Electronic Science and Technology of China, Chengdu, China, in 2004, and the Ph.D. degree from the City University of Hong Kong in 2011. From 2004 to 2006, he was a Research Engineer with Comba working on RF repeater system. From 2007 to 2008, he was a Research Assistant with the City University of Hong Kong. He joined the Institute for Infocomm Research, Singapore, as a Research Fellow and later served as a Scientist from 2011 to 2013. In 2013, he joined the School of Electronics and Information, Nantong University, China, as a Professor. His current research interests are RF/microwave components and subsystems, differential circuit and antennas, and LTCC circuits and antennas. He is the recipient of the IES Prestigious Engineering Achievement Award in 2013. He has served as a TPC member and the session chair for a number of conferences and a Regular Reviewer for the IEEE TRANSACTIONS ON MICROWAVE THEORY AND TECHNIQUES, the IEEE MICROWAVE AND WIRELESS COMPONENTS LETTERS, the IEEE ANTENNAS AND WIRELESS PROPAGATION LETTERS, *Electronic Letters*, and other publications.

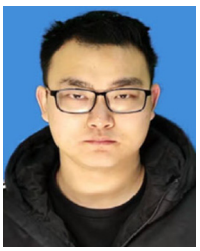

GU LIU was born in Yancheng, Jiangsu, China, in 1997. He received the B.Sc. degree from Nantong University, Nantong, Jiangsu, China, in 2019, where he is currently pursuing the M.S. degree in electromagnetic field and microwave technology. His current research interests include microwave antenna design.

KAI XU (Member, IEEE) was born in Haian, Jiangsu, China, in 1991. He received the B.Sc. degree from the Taizhou Institute of Science and Technology, Jiangsu, China, in 2013, and the M.S. and Ph.D. degrees from Nantong University, Nantong, Jiangsu, China, in 2016 and 2019, respectively. From 2015 to 2016, he was a Research Assistant with the Institute for Infocomm Research, Singapore. His current research interests include microwave components, balanced microwave circuits, antennas, and integrated designs. He is a Regular Reviewer of the IEEE TRANSACTIONS ON INDUSTRIAL ELECTRONICS, the IEEE MICROWAVE AND WIRELESS COMPONENTS LETTERS, the IEEE ACCESS, *IET Electronic Letters*, and other publications.